Journal of Solid State Chemistry **164,** 100–110 (2002)
doi:10.1006/jssc.2001.9504, available online at http://www.idealibrary.com on IDEAL®

Variations of the $FeGa_3$ Structure Type in the Systems $CoIn_{3-x}Zn_x$ and $CoGa_{3-x}Zn_x$

Per Viklund,* Sven Lidin,† Pedro Berastegui,† and Ulrich Häussermann†,[1]

*Department of Inorganic Chemistry 2, Lund University, S-22100 Lund, Sweden; and †Department of Inorganic Chemistry, Stockholm University, S-10691 Stockholm, Sweden

Received September 18, 2001; in revised form December 26, 2001; accepted January 4, 2002

We present an investigation of the quasibinary systems $CoIn_{3-x}Zn_x$ and $CoGa_{3-x}Zn_x$ which were structurally characterized by X-ray diffraction experiments and, in the case of $CoGa_{3-x}Zn_x$, additionally by neutron powder diffraction experiments. The limiting compositions were found to be $x = 0.81(2)$ and $x = 0.73(2)$ for $CoIn_{3-x}Zn_x$ and $CoGa_{3-x}Zn_x$, respectively. The isotypic binary compounds $CoIn_3$ and $CoGa_3$ crystallize with the $FeGa_3$ structure type (tetragonal, space group $P4_2/mnm$, $Z = 4$) in which the *p*-block atoms form an array of columns of centered cubes defined by two different crystallographic sites. The substitution of In or Ga by Zn takes place in an ordered fashion and produces "colored" variants of the $FeGa_3$ parent structure: In both systems Zn enters exclusively the position corresponding to the cube centers. Additionally, in $CoIn_{3-x}Zn_x$ this position is substituted in such a way that for a composition $CoIn_{2.5}Zn_{0.5}$, columns of Zn- and In-filled In_8 cubes along the *c* axis alternate. The latter substitution pattern is accompanied by a symmetry lowering of the parent $FeGa_3$ structure: The structure of $CoIn_{3-x}Zn_x$ is described by the space group $P4_2/m$ in which the cube center position is split into two separate sites. By performing first-principles electronic structure calculations we investigated the general bonding situation of the compounds $CoIn_3$ and $CoGa_3$ and the particular electronic effect when incorporating Zn. With respect to the density of states of the binary compounds the exchange of Ga or In by Zn virtually affects only the electronic states just below the Fermi level. On increasing Zn concentration a dip is created in the density of states which approximately coincides with the location of the Fermi level for an electron count corresponding to limiting composition of the two systems.

1. INTRODUCTION

Binary compounds formed between transition metals from the groups V–Co (*T*) and the group 13 *p*-block elements Al and Ga (*E*13)—exhibit distinct bonding and transport properties for low concentrations *T* (i.e., $E/T \geq 2$) (1–5). These properties coincide with a semimetallic behavior and originate from the presence of a broad pseudo gap at or close to the Fermi level in the density of states (DOS) in the T_m $(E13)_n$ compounds (5, 6). The pseudo gap is a consequence of strong directional (covalent) interactions between *T* and *E*13 atoms and separates *d–p* bonding from antibonding states. As a matter of fact, in some cases (e.g., in $RuAl_2$ (1), $RuGa_2$ (2), $FeGa_3$ (7) and $RuGa_3$ (7)) *T–E* interactions are so strong that instead of a pseudo gap, a real bandgap is opened at the Fermi level. This creates a peculiar class of narrow-bandgap semiconductors composed exclusively of good metallic conducting elements (7). Naturally, the presence of the pseudo gap in the DOS implies that these particular binary T_m $(E13)_n$ compounds are intermetallic electron compounds (8) where the electron count or valence electron concentration (VEC, number of valence electrons per formula unit) determines decisively the total energy, and other factors, such as size and electronegativity, are not very important.

We have started to systematically study the variation of binary electron compounds T_m $(E13)_n$ in ternary systems $T_m(E13)_{n-x}Zn_x$ to determine their stability ranges *x* (optimum electron counts) and to identify and characterize new structural representatives that do not occur among the binary systems. Besides the interesting bonding properties of these compounds we also focused on investigating the ordering tendencies of the two kinds of metals, *E*13 and Zn, on different sublattices. In particular we could establish the compound series $V_8Ga_{41} \rightarrow V_8Ga_{36.9}Zn_{4.1} \rightarrow Cr_8Ga_{29.8}Zn_{11.2} \rightarrow Mn_8Ga_{27.4}Zn_{13.6}$ with the V_8Ga_{41} structure type, which exposed a startling segregation of Zn and Ga leading to the formation of separated Zn_{13} cluster entities (9, 10). The Zn content of the phases is dependent on the transition metal *T*: the more electron rich *T* the more Zn is

[1]To whom correspondence should be addressed. Fax: +46-8-152187. E-mail: ulrich@inorg.su.se.

0022-4596/02 $35.00

incorporated into the corresponding phase $T_8(E13)_{41-x}Zn_x$. As a consequence, the electron count attains a very similar value for all compounds, provided that Zn only contributes to bonding by its 4*s* electrons. Thus, the different compositions of the compounds reflect the requirement of an optimum electron concentration for a stable V_8Ga_{41}-type structure, which is determined by the location of the pseudo gap in the DOS. In this article we report on the structural and electronic effects of the substitution of *E*13 by Zn in the systems $Co(E13)_{3-x}Zn_x$ (*E*13 = Ga, In). The binary compounds $CoGa_3$ and $CoIn_3$ are isotypic and crystallize with the $FeGa_3$ structure type.

2. EXPERIMENTAL

2.1. Synthesis and Compositional Analysis

The phases $Co(E13)_{3-x}Zn_x$ (*E*13 = In, Ga) were prepared from the pure elements (Co powder (Kebo, >99.5%), In granules (ABCR >99.9999%), Ga rod (ABCR, >99.9999%), and Zn granules (ABCR, >99.99%)). Syntheses were performed in two different ways. In one series we used mixtures with the compositions $Co(E13)_{10-x}Zn_x$ ($x = 1, 2, 3, 4, 5$) thus employing *E*13/Zn as reactant and flux medium. The other series consisted of stoichiometric mixtures with the compositions $Co(E13)_{3-x}Zn_x$ ($x = 0, 0.25, 0.5, 0.75, 1$). The reactants were carefully mixed, pressed into pellets, and loaded into quartz ampoules, which were sealed under vacuum (approx. 10^{-4} atm). All samples were heated to 900°C at 200°C/h, held at this temperature for 24 h, and finally cooled to room temperature at the rate of 20°C/h. Excess *E*13/Zn metal was dissolved with 3M HCl and the remains were washed with deionized water. All products in the systems examined consisted of shiny, silvery-gray crystals. The products were characterized by Guinier powder diagrams (Cu$K\alpha$; Si standard) and their compositions determined with the EDX (energy-dispersive X-ray) method in a JEOL JSM-840A Scanning Electron Microscope by averaging the compositions of between 5 and 10 crystallites for each sample.

2.2. Structure Determination

X-Ray investigations. A Huber Guinier G670 image foil powder camera with monochromatized Cu$K\alpha$ radiation was used for the collection of powder diffractograms (at room temperature). Silicon (SICOMILL, Kema Nord, Nobel Industries, Sweden) was used as internal standard. Lattice parameters were obtained from least-squares refinements of the measured and indexed lines of these powder diagrams (program PIRUM (11)). Single-crystal intensity data were collected from one crystal from each of the following samples $Co(E13)_3$, $CoGa_{2.75}Zn_{0.25}$, $CoIn_{2.5}Zn_{0.5}$, $Co(E13)_2Zn$ (nominal (synthesis) compositions) on a Siemens SMART CCD system (12) at room temperature with monochromatized Mo$K\alpha$ radiation (0.71073 Å). The data collection nominally covered a full sphere of reciprocal space. In each case data were corrected for Lorentzian polarization (13), extinction, and absorption (assuming a spherical crystal) (14). The structures were refined against F^2 using SHELXTL (15).

Neutron investigations. A neutron diffraction experiment was performed on the Polaris powder diffractometer at the ISIS facility, United Kingdom, with the sample encapsulated inside a thin-walled vanadium can. Time-of-flight diffraction data were collected from a sample $CoGa_{2.75}Zn_{0.75}$ (nominal composition) at room temperature using the backscattering detector bank which covers the scattering angles $135° < \pm 2\theta < 160°$ and provides data over the *d*-spacing range $0.5 < d < 3.2$ Å with a resolution $\Delta d d^{-1} = 5 \times 10^{-3}$. Rietveld profile refinements using the normalized diffraction data were performed with the program GSAS (16).

2.3. Electronic Structure Calculations

The electronic structures of tetragonal $Co(E13)_3$, $Co(E13)_{2.5}Zn_{0.5}$, and $Co_2(E13)_2Zn$ were calculated by the full-potential linearized augmented plane wave (FLAPW) method as provided in the program package WIEN97 (17). The space was divided into so-called muffin-tin spheres (MTS) surrounding atomic sites and interstitial regions between them. In full-potential techniques within density functional theory basis functions, electron densities and potentials are calculated without any shape approximation. We used well-converged plane wave sets with a cutoff parameter $R_{mt}K_{max} = 8.0$. The Co 3*p*, In 4*d*, and Ga and Zn 3*d* states were treated as local orbitals. Further the local density approximation (LDA) with the exchange-correlation potential parametrization according to Perdew *et al.* (18) was applied. Reciprocal space integrations were performed with the tetrahedron method (19) using $1000\,k$ points in the full Brillouin zone.

3. THE $FeGa_3$ STRUCTURE TYPE

Compounds with the $FeGa_3$ structure type (tetragonal, space group $P4_2/mnm$, $Z = 4$) are formed exclusively between a transition metal from either the Fe or Co group and one of the *E*13 metals Ga and In. The following eight compounds are known: $FeGa_3$, $RuGa_3$, $OsGa_3$, $CoGa_3$, $RuIn_3$, $CoIn_3$, $RhIn_3$, and $IrIn_3$ (20–22). Thus, VEC is confined to a range between 17 and 18 valence electrons per formula unit. The $FeGa_3$ structure contains as an important motif, the 3^2434 net (Fig. 1a), formed by one kind of Ga atoms (Wyckoff site 8*j*). This net has square

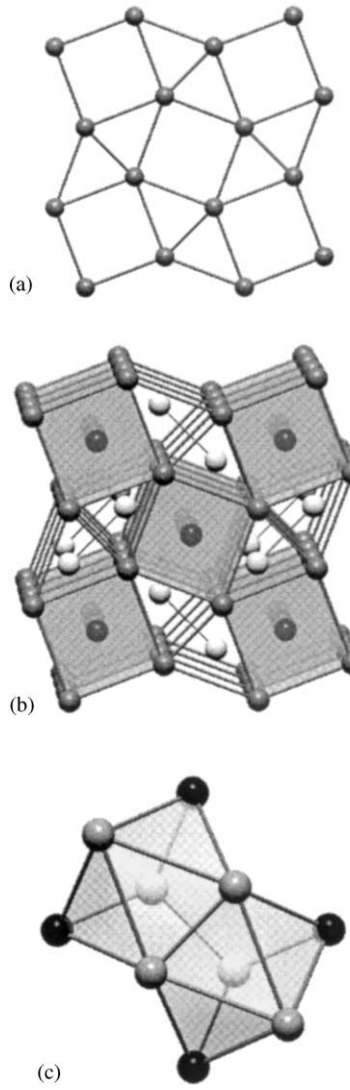

FIG. 1. Description of the tetragonal $FeGa_3$ structure. (a) The 3^2434 net formed by one kind of Ga atoms. (b) Stacking 3^2434 nets on top of each other generates rows of Ga_8 cubes (gray) and Ga_8 rhombic prisms. The cubes are centered by the second kind of Ga atoms; half of the rhombic prisms are occupied by pairs of Fe atoms (white circles). (c) The building block Fe_2Ga_{12}. The $FeGa_3$ structure is obtained from such units exclusively sharing corners. Fe atoms, white circles, 3^2434 net-forming Ga atoms, gray circles, cube-centering Ga atoms, black circles.

symmetry and can be obtained from the square 4^4 net by simply shearing half of the squares to diamonds (23). On stacking the 3^2434 nets on top of each other along the *c* direction a tetragonal assembly of columns of cubes and rhombic prisms (equivalent to two trigonal prisms sharing a square face) is formed (Fig. 1b). The cubes are centered by the second kind of Ga atoms (Wyckoff site 4*c*) whereas half of the rhombic prisms are occupied by pairs of Fe atoms (Wyckoff site 4*f*). The coordination polyhedron of a Fe atom is an all-square-face capped trigonal prism. Alternatively, the structure can be built up from units Fe_2Ga_{12} (Fig. 1c) which exclusively share corners, i.e., within the *ab* plane via the atoms capping the square faces of the trigonal prisms and in the *c* direction via atoms forming the trigonal prisms.

The electronic structures of $CoGa_3$ and $CoIn_3$ are similar, as presented in the DOS shown in Fig. 2. First, the overall shape is characteristic of T_m $(E13)_n$ electron compounds (5, 6): At low energy the density of states is dominated by approximately parabolically distributed nearly free-electron-like states stemming from the *sp* bands of the *E*13 substructure. At higher energy the *d* states of the Co atoms hybridize strongly with the *E*13 *p* bands. As a consequence of the Co(*d*)–*E*13(*p*) interactions the *T d* band is split into several parts. The part lowest in

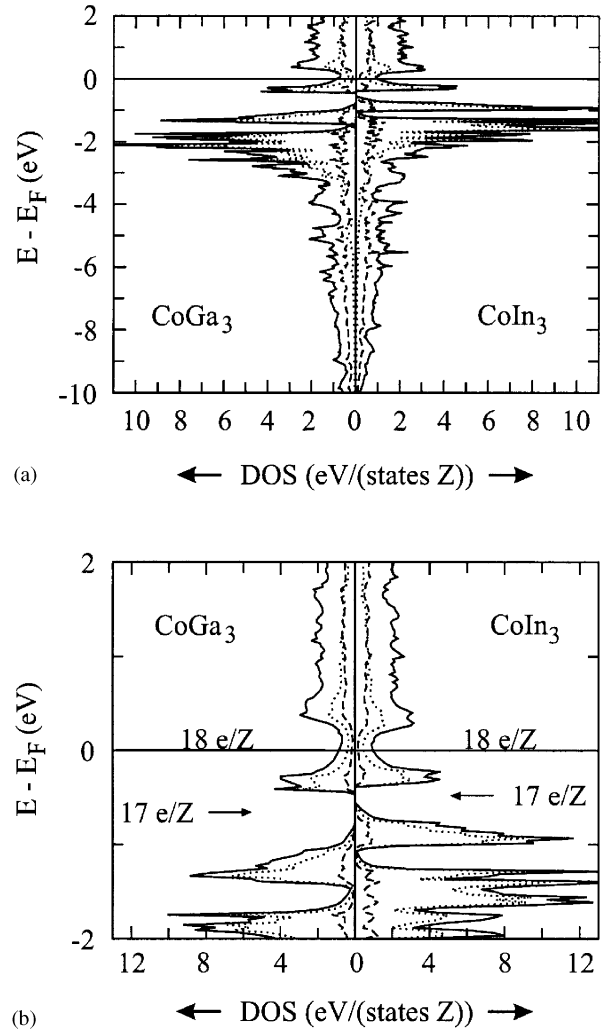

FIG. 2. (a) Total density of states (DOS (states/eV *Z*)) together with the Co (dotted lines) and E (broken lines) partial DOS for the compounds $CoGa_3$ and $CoIn_3$. (b) Closeup of the DOS for $CoGa_3$ and $CoIn_3$ for the states around the Fermi level. For an electron count of 17 electrons per formula unit (*Z*) the Fermi level becomes situated at a real bandgap.

energy with the largest dispersion (between −3.5 and −1.7 eV below the Fermi level for $CoGa_3$ and between −2.7 and −1.3 eV for $CoIn_3$) corresponds to strongly Co–*E*13 bonding states, whereas the two consecutive parts with narrow dispersion (at −1.2 and −0.5 eV for $CoGa_3$ and at −1 eV and −0.5 eV for $CoIn_3$) correspond to mainly nonbonding states. The Fermi level for both compounds is located in a pseudo gap separating the nonbonding (Co *d*-based) states from antibonding (hybridised Co *d*/*E*13 *p*) states. Importantly, the band structure of $CoGa_3$ displays a rigid-band behavior when compared with that of $FeGa_3$, which is a 17-electron compound (7). Thus, for $FeGa_3$ the Fermi level is put at the real bandgap between the two nonbonding, confined, *d* bands in the DOS which turns $FeGa_3$ into a narrow-bandgap semiconductor. Our original idea was to exchange Ga and In in $CoGa_3$ and $CoIn_3$ by Zn until a composition $Co(E13)_2Zn$, to obtain ternary 17-electron compounds with semiconductor properties.

4. THE SYSTEM $CoIn_{3-x}Zn_x$

The results of the syntheses are compiled in Table 1. When preparing $CoIn_{3-x}Zn_x$ from mixtures with excess (In/Zn), i.e., $CoIn_{10-x}Zn_x$ ($x = 1, 2, 3, 4, 5$), the composition of the product varies just slightly from $CoIn_{2.24(2)}Zn_{0.76(2)}$ to $CoIn_{2.19(2)}Zn_{0.81(2)}$ with increasing Zn content of the synthesis mixture. Synthesis from stoichiometric mixtures $CoIn_{3-x}Zn_x$ ($x = 0$, 0.25, 0.5, 0.75, 1) yielded products with somewhat lower Zn content than the nominal composition of the corresponding synthesis mixtures. For a synthesis mixture $CoIn_2Zn$ the product composition was the same as for the excess (In/Zn) synthesis mixture $CoIn_5Zn_5$ with the highest Zn content, i.e., $CoIn_{2.19(2)}Zn_{0.81(2)}$. Thus, we consider this composition as the homogeneity range border of quasibinary $CoIn_{3-x}Zn_x$.

4.1. Structure Refinement

Structure refinement of $CoIn_3$ single-crystal intensity data was performed in the space group $P4_2/mnm$ using the atomic position parameters previously obtained by Pöttgen *et al.* (22). The results are virtually identical. Measurement of a crystal from the sample with the nominal composition $CoIn_{2.5}Zn_{0.5}$ displayed a large number of weak reflections in violation of the systematic absences of the space group 136, $P4_2/m\ 2_1/n\ 2/m$; specifically, the (equivalent) conditions ($0kl$: $k + l = 2n$) and ($h0l$: $h + l = 2n$) corresponding to the *n*-glides perpendicular to the *a* and *b* axes were not fulfilled. Also the weaker subconditions ($0k0$: $k = 2n$) and ($h00$: $h = 2n$) were violated, obviating the 2_1 screws along *a* and *b*. The Laue class was, however, clearly $P4/mmm$ from the intensity distribution. This contradiction may be resolved if the possibility of twinning is considered. Lowering the Laue class to $P4/m$ introduces a possible direct type I subgroup solution, $P4_2/m$, that is not associated with extinction conditions emanating from operations with principal directions perpendicular to the tetrad, and further, it splits one of the In/Zn orbits into two separate positions, thus allowing In/Zn ordering. Domain twinning according to the matrix $[010\,100\,00\bar{1}]$ would then restore the apparent Laue symmetry $P4/mmm$. This mechanism seems quite likely, since the crystal may be considered effectively single with respect to the continuous $CoIn_2$ network, while twinning is caused by the local nature of Zn/In ordering in the $In_{0.5}Zn_{0.5}$ substructure. Single-crystal X-ray data from the sample $CoIn_{2.5}Zn_{0.5}$ were refined as a twinned structure in the space group $P4_2/m$. The refinement converged rapidly, and the structure shows a clear separation between Zn and In. In $P4_2/m$ the centers of the cubes are defined by the Wyckoff sites 2*a* and 2*b*. Refinement of the In/Zn occupancies for these sites yielded 85.1(9)% In/14.9(9)% Zn and 11.6(9)% In/88.4(9)% Zn, respectively. The site 8*k* defining the 3^2434 net remained fully occupied by In. Thus, the crystal composition amounts to $CoIn_{2.50(1)}Zn_{0.50(1)}$ which is somewhat higher than the average composition of the sample. The same procedure was then applied to data from the Zn-richest sample with the nominal composition $CoIn_2Zn$ and the occupancies of sites 2*a* and 2*b* were refined to 28(1)% In/72(1)% Zn and 25(1)% In/75(1)% Zn, respectively. Again, site 8*k* corresponded to a fully occupied In position, which gives a total composition of $CoIn_{2.27(2)}Zn_{0.73(2)}$ for the crystal, i.e., somewhat lower than the average composition of the sample ($CoIn_{2.19(2)}Zn_{0.81(2)}$). Interestingly, although the In/Zn distribution on the cube centering positions is almost the same, the symmetry lowering $P4_2/mnm \rightarrow P4_2/m$ is still apparent; however, the effects are much less pronounced. Some details of the single-crystal data collections and refinements are listed in Table 2. Atomic position parameters are given in Table 3, and selected interatomic distances in Table 4. Further details of the crystal structure investigation may be obtained from Fachinformationszentrum Karlsruhe, D-76344 Eggenstein-Leopoldshafen, Germany (fax: (+49)

TABLE 1
Nominal (Synthesis) Compositions and Actual Product Compositions (Obtained from EDX Analyses) of $CoIn_{3-x}Zn_x$

Nominal composition	EDX composition
$CoIn_{10-x}Zn_x$, $x = 1,2,3,4,5$	0.76(2)–0.81(2)
$CoIn_{2.75}Zn_{0.25}$	0.17(3)
$CoIn_{2.5}Zn_{0.5}$	0.42(7)
$CoIn_{2.25}Zn_{0.75}$	0.67(9)
$CoIn_2Zn_1$	0.81(3)

7247-808-666; e-mail: crysdata@fiz-karlsruhe.de) on quoting Depository Nos. CSD-412062 ($CoIn_3$), CSD-412066 ($CoIn_{2.5}Zn_{0.5}$), and CSD-412065 ($CoIn_{2.27}Zn_{0.73}$).

4.2. Variations in the Crystal Structure

The important changes in the $FeGa_3$ structure of $CoIn_3$ on substitution of In by Zn in the system $CoIn_{3-x}Zn_x$ are summarized in Fig. 3 (see also Table 4). The exchange of In by Zn takes place in a remarkably highly ordered fashion. First, Zn only enters the position of the cube centers and additionally this position is substituted in such a way that for a composition $CoIn_{2.5}Zn_{0.5}$ columns of Zn-filled In_8 cubes along the *c* axis alternate with In-filled ones. As a consequence, the space group symmetry is reduced to $P4_2/m$. Apart from the differently occupied cube centers the symmetry reduction is also recognized in a distortion of the 3^2434 net. In the lower symmetric space group this net may be composed of two differently sized squares. This allows the generation of columns of cubes of different size and, thus, a 'breathing' of the structure to accomodate differently sized Zn and In atoms in the same kind of coordination polyhedron. The breathing of the structure, which is supported by the ability of the 3^2434 net to corrugate (this, however, is not a consequence of the symmetry lowering), is especially pronounced for the composition $CoIn_{2.5}Zn_{0.5}$ (Fig. 3b). For higher Zn contents the In/Zn occupancies for the cube centering sites equalize, but since the size difference between Zn and In is quite pronounced slight differences in the occupancies (i.e., in our crystal with the composition $CoIn_{2.27(2)}Zn_{0.73(2)}$; cf. Table 3) still yield differently sized cubes and thus a recognizable symmetry lowering (Fig. 3c). The trend in the lattice parameters with increasing Zn content is shown in Fig. 4. The *a* and *c* parameters decrease by approximately the same amount. In the concentration range of the superstructure formation ($x<0.5$) the decrease appears somewhat larger than above.

5. THE SYSTEM $CoGa_{3-x}Zn_x$

The results of the syntheses are compiled in Table 5. When preparing $CoGa_{3-x}Zn_x$ from mixtures with excess (Ga/Zn), i.e., $CoGa_{10-x}Zn_x$ ($x=1$, 2, 3, 4, 5), the composition of the product varies just slightly from $CoGa_{2.75(1)}Zn_{0.25(1)}$ to $CoGa_{2.71(1)}Zn_{0.29(1)}$ with increasing Zn content of the synthesis mixture. Synthesis from stoichiometric mixtures $CoGa_{3-x}Zn_x$ (x = 0, 0.25, 0.5,

TABLE 2
X-Ray Single-Crystal Refinement Data for $CoIn_{3-x}Zn_x$

Composition	$CoIn_3$	$CoIn_{2.38(7)}Zn_{0.42(7)}$	$CoIn_{2.19(3)}Zn_{0.81(3)}$
Crystal system	Tetragonal	Tetragonal	Tetragonal
Space group	$P4_2/mnm$	$P4_2/m$	$P4_2/m$
Pearson symbol	*tP*16	*tP*16	*tP*16
a (Å)	6.8343(3)	6.7255(5)	6.6975(6)
c (Å)	7.0922(8)	7.0087(7)	6.9960(12)
V (Å^3)	331.26(4)	317.02(5)	313.82(7)
Z	4	4	4
ρ_{calcd} (g cm−1)	8.088	7.934	7.774
Crystal size (μm^3)	50 × 63 × 100	50 × 50 × 50	113 × 113 × 113
Transmission (max:min)	4.45	1.61	14.8
μ (mm^{-1})	25.237	26.516	26.854
2θ range *hkl*	8.3–63.0	5.8–62.6	5.8–62.6
Index range *hkl*	$-9\le h\le 9$	$-9\le h\le 9$	$-9\le h\le 9$
	$-8\le k\le 9$	$-9\le k\le 9$	$-9\le k\le 9$
	$-9\le l\le 10$	$-10\le l\le 5$	$-7\le l\le 9$
Total No. reflections	3109	3174	3165
R_{int}	0.0465	0.0268	0.0349
Independent reflections	322	531	532
Reflections with $I>2\sigma(I)$	275	479	486
Final *R* indices [$I>2\sigma$ (*I*)]	$R=0.0287$	$R=0.0233$	$R=0.0318$
	$wR=0.0605$	$wR=0.0563$	$wR=0.0969$
R indices (all data)	$R=0.0358$	$R=0.0271$	$R=0.0342$
	$wR=0.0626$	$wR=0.0578$	$wR=0.0983$
Extinction coefficient	0.152(5)	0.0093(6)	0.0265(18)
Largest diff. peak/hole (*e* Å^{-3})	1.611/−1.901	1.210/−1.043	1.354/−1.342

Note. The listed compositions were obtained from EDX analyses of the bulk samples and the lattice parameters from X-ray powder data.
[a] $R_1=\sum||F_o|-|F_c||/\sum|F_o|$. $wR_2=(\sum[w(F_o^2-F_c^2)^2])/(\sum[w(F_o^2)^2])$, $w=1/[\sigma^2(F_o^2)+(aP)^2+bP]$ and $P=(F_o^2+2F_c^2)/3$. $CoIn_3$ ($a=0.0306$, $b=2.63$), $CoZn_{0.4(1)}In_{2.6(1)}$ ($a=0.0303$, $b=1.01$), $CoZn_{0.9(1)}In_{2.1(1)}$ ($a=0.0418$, $b=4.26$)

TABLE 3
Atomic Position Parameters, Site Occupancies, and Isotropic Thermal Displacement Parameters for $CoIn_{3-x}Zn_x$

Atom	$P4_2/mnm$	x	y	z	s.o.f.	U_{eq}
			$CoIn_3$			
Co	4*f*	0.3500(1)	0.3500(1)	0	1	83(3)
In1	4*c*	0	0.5	0	1	155(2)
In2	8*j*	0.1546(1)	0.1546(1)	0.2551(1)	1	149(2)
	$P4_2/m$		$CoIn_{2.50(1)}$	$Zn_{0.050(1)}$		
Co	4*j*	0.1487(2)	0.3511(2)	0	1	66(2)
M1	2*a*	0	0	0	0.851(9) In 0.149 Zn	132(3)
M2	2*b*	0.5	0.5	0	0.116(9) In 0.884 Zn	156(4)
In	8*k*	0.1699(1)	0.6500(1)	0.2412(1)	1	133(2)
			$CoIn_{2.27(2)}Zn_{0.73(2)}$			
Co	4*j*	0.1486(3)	0.3525(3)	0	1	89(3)
M1	2*a*	0	0	0	0.28(1) In 0.72 Zn	139(5)
M2	2*b*	0.5	0.5	0	0.25(1) In 0.75 Zn	184(6)
In	8*j*	0.1645(1)	0.6597(1)	0.2395(1)	1	168(3)

Note. U_{eq} ($\times 10^4$ A^2) is defined as one-third of the trace of the orthogonalized U_{ij} tensor. The listed crystal compositions correspond to the refined site occupancies.

TABLE 4
Interatomic Distances (in Å) Calculated with the Lattice Parameters Obtained from X-Ray Powder Data of $CoIn_{3-x}Zn_x$

$CoIn_3$				$CoIn_{2.50(1)}Zn_{0.50(1)}$				$CoIn_{2.27(2)}Zn_{0.73(2)}$			
Co:	2	In1	2.602	Co:	1	M1	2.565	Co:	1	M1	2.552
	2	In2	2.616		1	M2	2.566		1	M2	2.560
	4	In2	2.711		2	In	2.571		2	In	2.562
	1	Co	2.900		2	In	2.630		2	In	2.655
					2	In	2.729		2	In	2.686
In1:	2	Co	2.602		1	Co	2.830		1	Co	2.804
	4	In2	3.115								
	4	In2	3.156	M1:	2	Co	2.565	M1:	2	Co	2.562
	2	In1	3.546		4	In	3.115		4	In	3.036
					4	In	3.184		4	In	3.119
In2:	1	Co	2.616		2	M1	3.504		2	M1	3.498
	2	Co	2.711								
	1	In2	2.988	M2:	2	Co	2.566	M2:	2	Co	2.552
	2	In1	3.115		4	In	2.968		4	In	3.000
	2	In1	3.156		4	In	3.039		4	In	3.084
	1	In2	3.473		2	M2	3.504		2	M2	3.498
	1	In2	3.619								
	4	In2	3.658	In:	1	Co	2.571	In:	1	Co	2.560
					1	Co	2.630		1	Co	2.655
					1	Co	2.729		1	Co	2.686
					1	M2	2.968		1	M2	3.000
					1	M2	3.039		1	M2	3.036
					1	In	3.048		1	In	3.071
					1	M1	3.115		1	M1	3.084
					1	M1	3.184		1	M1	3.119
					1	In	3.381		1	In	3.352
					2	In	3.451		2	In	3.522
					1	In	3.627		2	In	3.583
					2	In	3.702		1	In	3.644

Note. SD are all equal to or less than 0.002 Å

0.75, 1) yielded products with higher Zn content. Similar to the $CoIn_{3-x}Zn_x$ system, the Zn content of the products was somewhat lower than the nominal composition of the corresponding synthesis mixtures. For a synthesis mixture $CoGa_2Zn$ the composition of the $CoGa_{3-x}Zn_x$ product was $CoGa_{2.27(2)}Zn_{0.73(2)}$. The Guinier powder diagram of this sample also revealed the presence of CoGa (probably with incorporated Zn). Thus, we consider $CoGa_{2.27(2)}Zn_{0.73(2)}$ as the limiting composition of quasi-binary $CoGa_{3-x}Zn_x$.

5.1. Structure Refinement

X-Ray single-crystal diffraction. Structure refinement of $CoGa_3$ single-crystal intensity data was performed in the space group $P4_2/mnm$ using the atomic position parameters obtained by Tao-Fan and Ching-Kwei from X-ray powder data (24). Our single-crystal refined atomic position parameters differ slightly from the literature data, but are more precise. Also, refinement of crystals from samples with the nominal composition $CoGa_{2.75}Zn_{0.25}$ and $CoGa_2Zn$ was undertaken in the space group $P4_2/mnm$ although the intensity data of the latter showed, as was the case for $CoIn_{3-x}Zn_x$ crystals, a number of reflections violating the systematic absence ($0kl$: $k+l=2n$) of the space group $P4_2/mnm$. However, refinement in the lower symmetric space group $P4_2/m$ yielded slightly higher residual values. The actual compositions of the two $CoGa_{3-x}Zn_x$ crystals were determined by EDX analysis after intensity data collection and found to be $CoGa_{2.76(1)}Zn_{0.24(1)}$ and $CoGa_{2.29(2)}Zn_{0.71(2)}$ for the Zn-poor and Zn-rich sample, respectively. Some details of the single-crystal data collections and refinements are listed in Table 6. Atomic position parameters are given in Table 7, and selected interatomic distances in Table 8. Further details of the crystal structure investigation may be obtained from Fachinformationszentrum Karlsruhe, D-76344 Eggenstein-Leopoldshafen, Germany (fax: (+49)7247-808-666; e-mail: crysdata@fiz-karlsruhe.de) on quoting Depository Nos. CSD-412061 ($CoGa_3$), CSD-412064 ($CoGa_{2.76}Zn_{0.24}$), and CSD-412063 ($CoGa_{2.29}Zn_{0.71}$).

Neutron powder diffraction. X-Ray diffraction studies are unable to discriminate between Zn ($Z=30$) and Ga ($Z=31$), whereas the neutron scattering lengths of those elements differ by about 20%. Thus, we used neutron diffraction to unequivocally extract the distribution of Zn and Ga atoms in the intermetallic framework. While

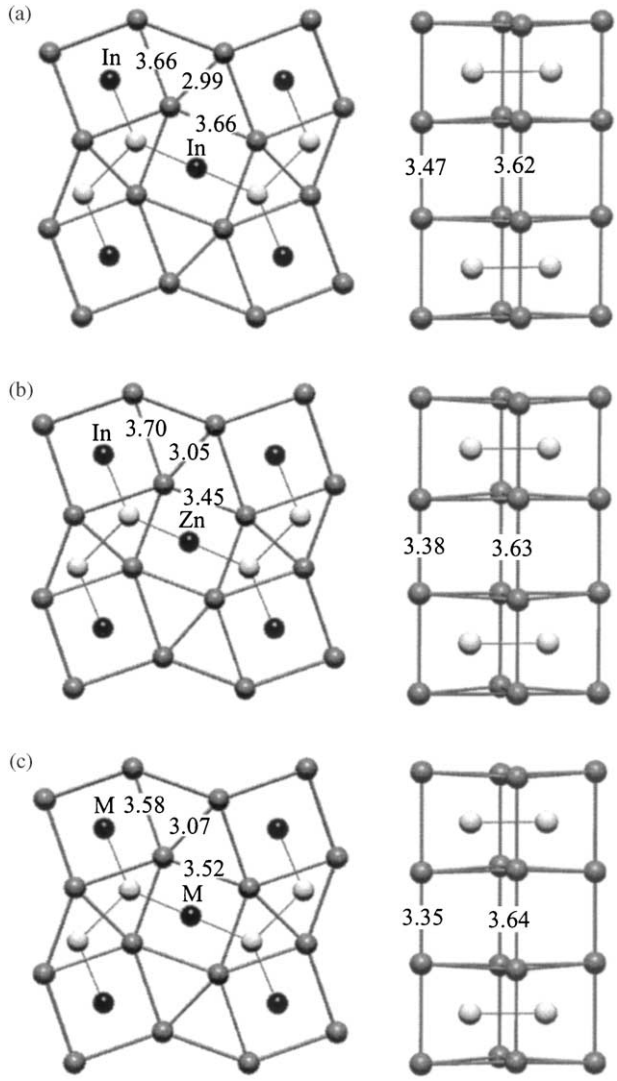

FIG. 3. Variation of the crystal structure in the system $CoIn_{3-x}Zn_x$. Left: Slab with half a unit cell thickness projected along [001]. Right: row of rhombic prisms occupied by pairs of Co atoms. $CoIn_3$ (a), Co_2In_5Zn (b), and $Co_2In_{2.25}Zn_{0.75}$(c). *M* indicates a Zn/In mixed occupied position with ≈ (75% Zn/25% In). Important distances (in Å) are included: Co atoms, white circles; 3^2434 net-forming In atoms, gray circles; cube-centering atoms, black circles.

refining the neutron powder data of a $CoGa_{2.25}Zn_{0.75}$ sample we found that it contained two additional phases, CoGa and a small amount of an as yet unidentified phase. The refined fractional weight of CoGa in the sample was 23%. A multiphase refinement was performed including six background parameters, an extinction correction parameter, and three profile parameters for each phase. Initial values for the Zn-doped $CoGa_3$ phase were obtained from the single-crystal X-ray diffraction experiment. The lattice parameters were $a = 6.31952(6)$ and $c = 6.2600(1)$ Å. The final refinement in the space group $P4_2/mnm$ included 30

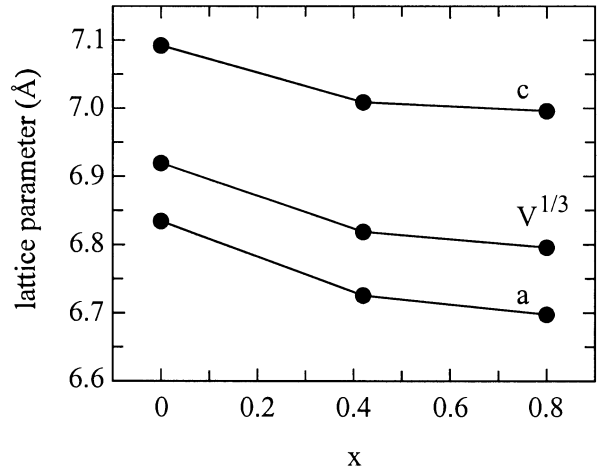

FIG. 4. Variation of the lattice parameters (obtained from X-ray powder data) and the cubic root of the cell volume in the system $CoIn_{3-x}Zn_x$ as a function of composition (x).

variables and converged with $R_{wp} = 2.8\%$ and $R_p = 4.9\%$. Further results are listed in Table 9. Zn was observed to enter the structure at the 4*c* (0, 0.5, 0) position only, and an attempt to refine the structure in $P4_2/m$ where this position is split into 2*a* (0, 0, 0) and 2*b* (0.5, 0.5, 0) was unstable. The Zn content of the phase $CoGa_{3-x}Zn_x$ corresponded to $x = 0.62(3)$ which is somewhat lower than the corresponding EDX- determined composition, $CoGa_{2.31(2)}Zn_{0.69(2)}$.

5.2. Variations in the Crystal Structure

As for $CoIn_{3-x}Zn_x$ in the $CoGa_{3-x}Zn_x$ system Zn was found to occupy exclusively the position of the cube centers of the parent $FeGa_3$ structure. Otherwise the incorporation of Zn into $CoGa_3$ has only a minor effect on crystal structure; the interatomic distances change only slightly (see Table 8). Since the atomic volumes of Zn and Ga are very similar this is not surprising. However, we are left with an important question: Are the cube centers substituted randomly by Zn or in the ordered fashion observed for the system $CoIn_{3-x}Zn_x$? Our diffraction experiments actually do not provide any information on this issue. The symmetry lowering $P4_2/mnm \rightarrow P4_2/m$ is caused by the

TABLE 5
Nominal (Synthesis) Compositions and Actual Product Compositions (Obtained from EDX Analysis) of $CoGa_{3-x}Zn_x$

Nominal composition	EDX composition
$CoGa_{10-x}Zn_z$, $x = 1,2,3,4,5$	0.25(1)–0.29(1)
$CoGa_{2.75}Zn_{0.25}$	0.24(2)
$CoGa_{2.5}Zn_{0.5}$	0.43(2)
$CoGa_{2.25}Zn_{0.75}$	0.69(2)
$CoGa_2Zn_1$	0.73(2)

TABLE 6
X-Ray Single-Crystal Refinement Data for $CoGa_{3-x}Zn_x$

Parameter	$CoGa_3$	$CoGa_{2.76(2)}Zn_{0.24(2)}$	$CoGa_{2.27(2)}Zn_{0.73(2)}$
Crystal system	Tetragonal	Tetragonal	Tetragonal
Space group	$P4_2/mnm$	$P4_2/mnm$	$P4_2/mnm$
Pearson symbol	$tP16$	$tP16$	$tP16$
a (Å)	6.2300(2)	6.2772(3)	6.3120(4)
c (Å)	6.4312(6)	6.3530(6)	6.2418(8)
V (Å^3)	249.61(3)	250.33(4)	248.68(4)
Z	4	4	4
ρ_{calcd} (g cm^{-1})	7.134	7.056	7.078
Crystal size (μm^3)	$75 \times 50 \times 50$	$88 \times 88 \times 88$	$200 \times 100 \times 113$
Transmission (maximum)	1.98	16.29	4.29
μ (mm^{-1})	38.155	37.455	37.453
2θ range hkl	9.1–62.9	5.8–62.6	5.8–62.6
Index range hkl	$-6 \le h \le 8$	$-9 \le h \le 9$	$-9 \le h \le 9$
	$-8 \le k \le 8$	$-9 \le k \le 9$	$-9 \le k \le 9$
	$-9 \le l \le 9$	$-10 \le l \le 5$	$-7 \le l \le 9$
Total No. reflections	2399	2279	2343
R_{int}	0.0352	0.0421	0.0450
Independent reflections	244	243	247
Reflections with $I > 2\sigma(I)$	195	216	232
Final R indices [$I > 2\sigma(I)$]	$R = 0.0235$	$R = 0.0337$	$R = 0.0352$
	$wR = 0.0492$	$wR = 0.0853$	$wR = 0.0904$
R indices (all data)	$R = 0.0354$	$R = 0.0364$	$R = 0.0374$
	$wR = 0.0512$	$wR = 0.0868$	$wR = 0.0916$
Extinction coefficient	0.048(2)	0.016(2)	0.068(6)
Largest diff. peak/hole (e Å^{-3})	1.126/−0.973	1.359/−1.378	1.643/−1.880

Note. The listed compositions were obtained from EDX analyses of the bulk samples and the lattice parameters from X-ray powder data.
[a] $R1 = \sum||F_o|-|F_c||/\sum|F_o|$. $wR_2 = (\sum[w(F_o^2-F_c^2)^2])/(\sum[w(F_o^2)^2])$, $w = 1/[\sigma_2(F_o^2) + (aP)^2 + bP]$ and $CoGa_3$ ($a = 0.0245$, $b = 0.00$), $CoZn_{0.4(1)}Ga_{2.6(2)}$ ($a = 0.0451$, $b = 1.73$), $CoZn_{0.7(1)}Ga_{2.3(1)}$ ($a = 0.0423$, $b = 1.77$).

breathing of the structure (differently sized cubes) and the different occupancies at the two cube centering sites. This has two consequences: first, and most important, reflections hkl and khl become non-symmetry equivalent, and second the conditions ($0kl$: $k + l = 2n$) and ($h00$: $h = 2n$) are raised. Since the breathing effect in the $CoGa_{3-x}Zn_x$ system is negligible the main contribution to the symmetry lowering will come just from the ordered occupation Ga/Zn. As a consequence, the intensity of the reflections allowed in $P4_2/m$ but forbidden in $P4_2/mnm$($0kl$: $k + l = 2n$) and ($h00$: $h = 2n$)) is very low. Finally, any intensity differences between the $P4_2/m$ inequivalent reflections hkl and khl are masked by their coinciding d values. Therefore, it was impossible to detect a symmetry lowering $P4_2/mnm \rightarrow P4_2/m$ in the refinement of our neutron powder data. However, it is likely that the incorporation of Zn into $CoGa_3$ is accompanied by superstructure formation as was found for $CoIn_{3-x}Zn_x$. Finally, the trend in the lattice parameters, as depicted in Fig. 5, is rather interesting. With increasing Zn content the a parameter increases whereas the c parameter decreases (the volume remains almost constant on substitution). This results in a cubic metric for the unit cell of tetragonal $CoGa_{3-x}Zn_x$ at a composition slightly above $x = 0.5$.

In conclusion we observe a clear segregation of Zn and the $E13$ metals in the systems $CoIn_{3-x}Zn_x$ and $CoGa_{3-x}Zn_x$. Additionally the segregation leads to a peculiar superstructure of the parent $FeGa_3$ structure type for concentrations $x \le 0.5$ in the $CoIn_{3-x}Zn_x$ system and possibly as well in the $CoGa_{3-x}Zn_x$ system. Coming back to our initial idea of preparing ternary 17-electron compounds with semiconducting properties we could not succeed in obtaining the desired compositions $Co(E13)_2Zn$. In the last step we examine the origin of the limiting composition of the systems $Co(E13)_{3-x}Zn_x$.

6. ELECTRONIC EFFECT OF THE ZN–(E13) SUBSTITUTION

To investigate the electronic effect of the exchange of $E13$ by Zn in $Co(E13)_3$ we calculated the DOS of $Co(E13)_3$, $Co(E13)_{2.5}Zn_{0.5}$ (space group $P4_2/m$), and $Co(E13)_2Zn$ (space group $P4_2/mnm$) in their experimentally determined crystal structures. For $Co(E13)_2Zn$ we used the lattice parameters of the respective Zn-richest compositions. The results are presented in Fig. 6. Note that the DOS curves are presented in such a way that the bottoms of the valence bands of all compounds within a series coincide. This

TABLE 7
Atomic Position Parameters, Site Occupancies, and Isotropic Thermal Displacement Parameters for $CoGa_{3-x}Zn_x$

Atom	$P4_2/mnm$	x	y	z	s.o.f.	U_{eq}
			$CoGa_3$			
Co	4*f*	0.3462(1)	0.3462(1)	0	1	47(3)
Ga1	4*c*	0	0.5	0	1	143(3)
Ga2	8*j*	0.1520(1)	0.1520(1)	0.2546(1)	1	132(2)
			$CoGa_{2.76(1)}Zn_{0.24(1)}$			
Co	4*f*	0.3469(1)	0.3469(1)	0	1	68(4)
M	4*c*	0	0.5	0	0.76(1) Ga 0.24 Zn	162(4)
Ga	8*j*	0.1536(1)	0.1536(1)	0.2564(1)	1	135(3)
			$CoGa_{2.29(2)}Zn_{0.71(2)}$			
Co	4*f*	0.3488(1)	0.3488(1)	0	1	113(4)
M	4*c*	0	0.5	0	0.29(2) Ga 0.71 Zn	216(4)
Ga	8*j*	0.1566(1)	0.1566(1)	0.2591(1)	1	165(4)

Note. U_{eq} ($\times 10^4$ A^2) is defined as one-third of the trace of the orthogonalized U_{ij} tensor. The listed crystal compositions correspond to the EDX-determined compositions on the actual single crystals.

TABLE 8
Interatomic Distances (in Å) Calculated with the Lattice Parameters Obtained from X-Ray Powder Data of $CoGa_{3-x}Zn_x$

$CoGa_3$				$CoGa_{2.76(2)}Zn_{0.24(2)}$				$CoGa_{2.27(2)}Zn_{0.73(2)}$			
Co:	2	Ga1	2.360	Co:	2	Ga	2.366	Co:	2	Ga	2.357
	2	Ga2	2.368		2	M	2.380		2	M	2.400
	4	Ga2	2.474		4	Ga	2.470		4	Ga	2.457
	1	Co	2.710		1	Co	2.719		1	Co	2.699
Ga1:	2	Co	2.360	M:	2	Co	2.380	N:	2	Co	2.400
	4	Ga2	2.844		4	Ga	2.838		4	Ga	2.817
	4	Ga2	2.877		4	Ga	2.883		4	Ga	2.879
	2	Ga1	3.216		2	M	3.170		2	M	3.121
Ga2:	1	Co	2.368	Ga:	1	Co	2.366	Ga:	1	Co	2.357
	2	Co	2.474		2	Co	2.471		2	Co	2.457
	1	Ga2	2.679		1	Ga	2.727		1	Ga	2.796
	2	Ga1	2.844		2	M	2.834		2	M	2.817
	2	Ga1	2.877		2	M	2.883		2	M	2.879
	1	Ga2	3.156		1	Ga	3.096		1	Ga	3.008
	1	Ga2	3.275		1	Ga	3.257		1	Ga	3.234
	4	Ga2	3.346		4	Ga	3.365		4	Ga	3.371

Note. SD are all equal to or less than 0.002 Å.

provides better comparability with respect to rigid band behavior. We recognize that both systems behave similarly under substitution. The incorporation of Zn affects the electronic states in a rather narrow range of -1 eV below the Fermi level when taking the DOS of $Co(E13)_3$ as reference. On depletion, the highest-lying occupied (non-bonding) band changes, whereas the remaining bands basically display rigid band behavior. The most important effect of Zn incorporation is that the bandgap in the DOS corresponding to an electron count of 17 in $Co(E13)_3$ closes, and for the hypothetical compositions $Co(E13)_2Zn$ the DOS at the Fermi level attains a considerably high value. This means that it would not have been possible to obtain ternary 17-electron semiconductors even if the compositions $Co(E13)_2Zn$ had been experimentally accessible.

A closer look at the evolution of the DOS curves on Zn–*E*13 substitution also reveals a possible explanation for the particular limiting compositions of the phases, which are very similar. The highest occupied band in $Co(E13)_3$ (the one that is depleted by the incorporation of Zn) is actually split. In the case of rigid band behavior the Fermi level would coincide with the small dip separating the peaks of the split for a band filling of 17.5 electrons (i.e., a composition $Co(E13)_{2.5}Zn_{0.5}$). However, the substitution process broadens the highest occupied band and it merges considerably with the neighboring ones for a composition $Co(E13)_2Zn$. (This broadening is much more pronounced in the $CoIn_{3-x}Zn_x$ system.) As a consequence, the Fermi levels for the compositions $Co(E13)_{2.5}Zn_{0.5}$ and $Co(E13)_2Zn$ appear at the peaks of the split. This is not a particularly favorable electronic situation. The electron count corresponding to the limiting composition of both systems (≈ 17.75) does, however, coincide with the dip in the DOS curves, as indicated by the dotted line in Fig. 6. Further, the pronounced double-peak structure of the highest occupied band in $CoGa_{2.5}Zn_{0.5}$ might explain the different compositions of $Co(E13)_{3-x}Zn_x$ when preparing the phases from a flux (i.e., with excess *E*13/Zn). For $CoGa_{3-x}Zn_x$ a composition $x = 0.29(1)$ was obtained where the Fermi level would be situatued above the the sharp peak which cuts the Fermi level in the DOS of $CoGa_{2.5}Zn_{0.5}$. For $CoIn_{3-x}Zn_x$, where this double-peak feature of the highest occupied band is rather weak, the composition obtained from the flux syntheses corre-

TABLE 9
Atomic Position Parameters, Site Occupancies, and Isotropic Thermal Displacement Parameters Obtained from the Rietveld Refinement of Neutron Powder Data of a Sample with Nominal Composition $CoGa_{2.25}Zn_{0.75}$

Atom	$P4_2/mnm$	x	y	z	s.o.f.	U_{eq}
Co	4*f*	0.3481(3)	0.3481(3)	0	1	78(4)
M	4c	0	0.5	0	0.38(3) Ga 0.62 Zn	95(2)
Ga	8*j*	0.1567(1)	0.1567(1)	0.2606(1)	1	124(4)

Note. U_{eq} ($\times 10^4$ Å^2) is defined as one-third of the trace of the orthogonalized U_{ij} tensor.

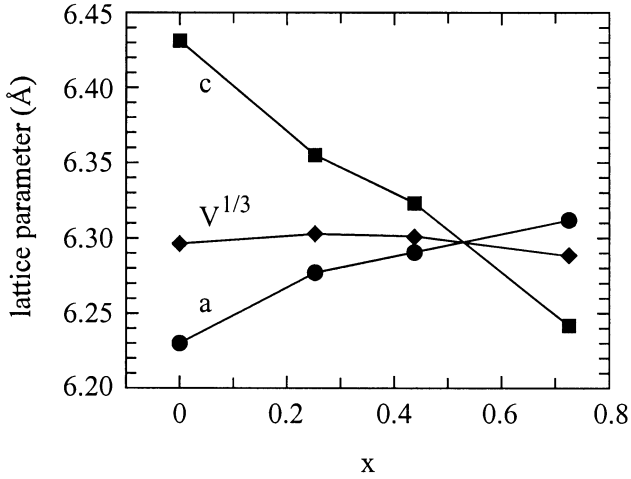

FIG. 5. Variation of the lattice parameters (obtained from X-ray powder data) and the cubic root of the cell volume in the system $CoGa_{3-x}Zn_x$ as a function of composition (x).

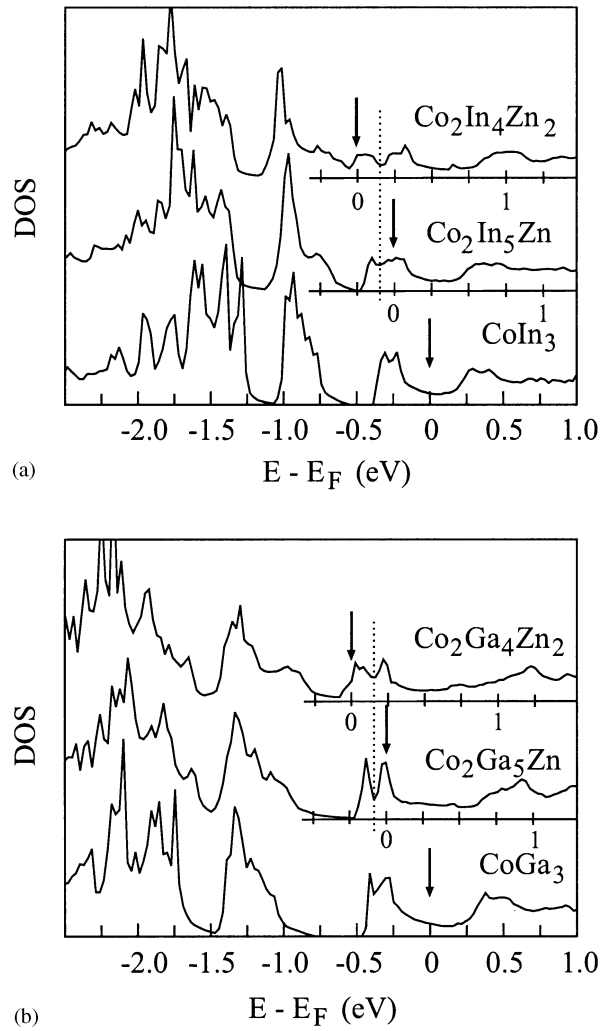

FIG. 6. Variation in the total density of states (DOS) (states/eV Z)) in the systems $CoIn_{3-x}Zn_x$ (a) and $CoIn_{3-x}Zn_x$ (b). For better comparability, the energy scale of the DOS curves for the Zn-substituted compounds is shifted so that the bottoms of the valence band of all three compounds are on top of each other. The Fermi levels are marked by arrows. The dotted lines indicate the position of the Fermi level (located in a dip of the DOS) for a composition $Co(E13)_{2.25}Zn_{0.75}$, corresponding approximately to the limiting composition of the phases $Co(E13)_{3-x}Zn_x$.

sponded to the limiting composition (i.e., $x \approx 0.8$, cf. Tables 1 and 5).

7. CONCLUSIONS

Compounds with the $FeGa_3$ structure type have a peculiar electronic structure with a bandgap at the Fermi level in the case of 17-electron compounds. Thus, one could assume that substitution of Ga or In by divalent Zn reduces the electron count in the 18-electron compounds $CoGa_3$ and $CoIn_3$ and produces ternary 17-electron compounds with semiconducting, or at least semimetallic, properties. However, it was not posssible to obtain compounds with the desired composition $Co(E13)_2Zn$ ($E13$ = Ga, In). Instead the limiting composition of the phases $Co(E13)_{3-x}Zn_x$ was found to be around $x = 0.8$. First-principle calculations could explain this fact as alteration of the highest occupied band in the band structures of $CoGa_3$ and $CoIn_3$ on depletion. Thus, rigid band behavior is not maintained while exchanging Ga or In by Zn. Nevertheless, the substitution experiments revealed interesting results from a structural point of view. In the $FeGa_3$ structure type of binary $CoGa_3$ and $CoIn_3$, the $E13$ atoms form an array of columns of centered cubes defined by two different crystallographic sites. The substitution of In or Ga by Zn takes place in an ordered fashion and produces "colored" variants of the $FeGa_3$ parent structure: In both systems there is a clear segregation of Zn and the $E13$ metals and Zn enters exclusively the position corresponding to the cube centers. Additionally, in $CoIn_{3-x}Zn_x$ this position is substituted in such a way that for a composition $CoIn_{2.5}Zn_{0.5}$ columns of Zn-filled In_8 cubes along the c axis alternate with In-filled ones. The latter substitution pattern is accompanied by a symmetry lowering of the parent $FeGa_3$ structure.

ACKNOWLEDGMENTS

This work was supported by the Swedish National Science Research Council (NFR) and the Göran Gustafsson Foundation. Additionally, we acknowledge a fund from the European Community through its Access to Research Infrastructure Action of the Improving Human Potential Program. We thank Steve Hull at ISIS Facility, Rutherford Appleton Laboratory, UK, for his assistance in performing the neutron diffraction experiments.

REFERENCES

1. D. Mandrus, V. Keppens, B. C. Sales, and J. L. Sarrao, *Phys. Rev. B* **58,** 3712 (1998).
2. J. Evers, G. Oehlinger, and H. Meyer, *Mater. Res. Bull.* **19,** 1177 (1984).
3. K. Yamamoto and Y. Matsuo, *J. Phys. Condens. Matter* **12,** 2359 (2000).
4. K. Yamamoto, M. Jono, and Y. Matsuo, *J. Phys. Condens. Matter* **11,** 1015 (1999).
5. U. Häussermann, P. Viklund, M. Boström, R. Norrestam, and S. I. Simak, *Phys. Rev. B* **63,** 125118 (2001).
6. G. Trambly de Laissardière, D. Nguyen Manh, L. Magaud, J. P. Julien, F. Cyrot-Lackmann, and D. Mayou, *Phys. Rev. B* **52,** 7920 (1995).
7. U. Häussermann, M. Boström, P. Viklund, Ö. Rapp, and T. Björnängen, *J. Solid State Chem.* **164,** 94 (2002).
8. R. Ferro and A. Saccone, *in*: "Materials Science and Technology" (R. W. Cahn, P. Haasen, and E. J. Kramer, Eds), Vol. 1: "The Structure of Solids." VCH, Weinheim, 1993.
9. U. Häussermann, P. Viklund, C. Svensson, S. Eriksson, P. Berastegui, and S. Lidin, *Angew. Chem. Int. Ed. Engl.* **38,** 488 (1999).
10. P. Viklund, C. Svensson, S. Hull, S. I. Simak, P. Berastegui, and U. Häussermann, *Chem. Eur. J.* **7,** 5143 (2001).
11. P.-E. Werner, *Ark. Kem.* **31,** 513 (1969).
12. Siemens Analytical X-Ray Instruments Inc., "SMART Reference Manual." Madison, WI, 1996.
13. Siemens Analytical X-ray Instruments Inc., "ASTRO and SAINT: Data Collection and Processing Software for the SMART System," Madison, WI, 1995.
14. G. M. Sheldrick, "SADABS, Program for Scaling and Correction of Area Detector Data," Univ. of Göttingen, Germany, 1996.
15. G. M. Sheldrick, "SHELXTL," Version 5.1., Bruker AXS, Madison, WI, USA, 1998.
16. A. C. Larson, R. B. von Dreele, and M. Lujan, "GSAS: The General Structure Analysis System." Los Alamos National Laboratory, Los Alamos, NM, 1994.
17. P. Blaha, K. Schwarz, and J. Luitz, "Program WIEN97: A Full Potential Linearized Augmented Plane Wave Package for Calculating Crystal Properties" (K. Schwarz, Techn. Universität Wien, 1999). ISBN 3-9501031-0-4.
18. J. P. Perdew, J. A. Chevary, S. H. Vosko, K. A. Jackson, M. R. Pederson, D. J. Singh, and C. Fiolhais, *Phys. Rev. B* **46,** 6671 (1992).
19. P. E. Blöchl, O. Jepsen, and O. K. Andersen, *Phys. Rev. B* **49,** 16223 (1994).
20. P. Villars and L. D. Calvert, "Pearsons Handbook of Crystallographic Data for Intermetallic Phases," 2nd ed. Am. Soc. for Metals, Materials Park, OH, 1991; Desk Edition, 1997.
21. R. Pöttgen, *J. Alloys. Compd.* **226,** 59 (1995).
22. R. Pöttgen, R.-D. Hoffmann, and G. Kotzyba, *Z. Anorg. Allg. Chem.* **624,** 255 (1998).
23. B. G. Hyde and S. Andersson, "Inorganic Crystal Structures," John Wiley, New York, 1989.
24. C. Tao-Fan and L. Ching-Wei, *Chin. Phys.* **22,** 701 (1967).